Estuaries and Coasts
Aug 2006, vol. 29(4): Pages 653-664

Tidally-induced shear stress variability above intertidal mudflats. Case of the macrotidal Seine estuary

Verney R. [1,2,*], Brun-Cottan J-C. [3], Lafite R. [1], Deloffre J. [1] and Taylor, J.A. [4]

(1) UMR CNRS 6143 M2C, University of Rouen, 76821 Mont Saint Aignan Cedex, FRANCE
(2) DYNECO-PHYSED, IFREMER, BP70, 29280 Plouzane, France
(3) UMR CNRS 6143 M2C, University of Caen, 24 Allée des Tilleuls, 14000 Caen, France
(4) Coastal and Estuarine Research Group, School of Life Sciences, University of Sussex, Falmer, Brighton, BN1 9QJ, U.K.

*: romaric.verney@ifremer.fr

Abstract:

Tidal currents and tidally-induced shear stress spatial variability were studied during a tidal cycle on four intertidal mudflats from the fluvial to the marine part of the Seine estuary. Measurements were carried out during low water discharge (<400 m3 s-1) in neap and spring tide conditions. Turbulent Kinetic Energy (TKE), Covariance (COV) and Logarithmic profile (LP) methods were used and compared for the determination of shear stress. The CTKE coefficient value of 0.19 cited in the literature was confirmed. Shear stress values were shown to decrease above mudflats from the mouth to the fluvial part of the estuary due to dissipation of the tidal energy, from 1N m-2 to 0.2N m-2 for spring tides and 0.8N m-2 to 0.05N m-2 for neap tides. Flood currents dominate tidally-induced shear stress in the marine and lower fluvial estuary during neap and spring tides and in the upper fluvial part during spring tides. Ebb currents control tidally-induced shear stress in the upper fluvial part of the estuary during neap tides. These results revealed a linear relationship between friction velocities and current velocities. Bed roughness length values were calculated from the empirical relationship given by Mitchener and Torfs [(1996) Erosion of mud/sand mixtures, Coastal Engineering, 29, 1-25] for each site; these values are in agreement with the modes of the sediment particle-size distribution. The influence of tidal currents on the mudflat dynamics of the Seine estuary was examined, by comparing the tidally-induced bed shear stress and the critical erosion shear stress estimated from bed sediment properties. Bed sediment resuspension induced by tidal currents was shown to occur only in the lower part of the estuary. Résumé

Keywords: Tidal currents, shear stress, intertidal mudflat, neap-spring conditions, spatial variability, Seine estuary (France)

NOMENCLATURE

Latin symbols

C_d: drag coefficient

C_{TKE}: best fit coefficient for K-τ_{TKE} conversion

E_1, E_2: empirical coefficients for the calculation of critical erosion shear stress

h (m): water height

K: Turbulent kinetic energy (m^2s^{-2})

kp (km): Location reference for the Seine, (kp0 is the Pont Marie, Paris)

u,v,w ($m.s^{-1}$): instantaneous current velocity components following the coordinates E,N,Up

$\overline{U}, \overline{V}, \overline{W}$ ($m.s^{-1}$): average current velocity components

u', v', w' ($m.s^{-1}$): fluctuating current velocity components

U(z) ($m.s^{-1}$): mean horizontal current velocity

u* ($m.s^{-1}$): friction velocity

W% : water content

z (m): recording height above the bed

z_0 (mm): bed roughness length

Greek symbols

α_F; α_E: U-u* best fit coefficients for ebb and flood stages

κ: Von Karman constant

ρ ($kg.m^{-3}$): Water density

ρ_b ($kg.m^{-3}$): sediment bulk density

τ_{ce} ($N.m^{-2}$): critical erosion shear stress

τ_{re} ($N.m^{-2}$): Reynolds shear stress

τ_{COV} ($N.m^{-2}$): Total shear stress obtained from the Reynolds shear stress

τ_{TKE} ($N.m^{-2}$): Turbulent kinetic energy shear stress

$\tau_{VISCOUS}$ ($N.m^{-2}$): Viscous shear stress

τ_{LP} ($N.m^{-2}$): ¨Shear stress calculated from the LP method

ν ($m^2.s^{-1}$): Kinematic viscosity of water

ξ: empirical constant for calculation of critical erosion shear stress

INTRODUCTION

Over the past twenty years, various studies have described how macrotidal estuarine systems vary with time and in space (Uncles et al., 1998; Dyer et al., 2000; Le Hir et al., 2000). Among all physical, chemical and biological gradients observed in estuaries, the hydrodynamic parameters are considered to be the most important forcing parameter for all micro and macro scale estuarine processes (Mikes et al., 2004). Hydrodynamic parameters are controlled by the seasonal fluvial discharge, tidal propagation and episodic energetic events such as swell, and wind- and vessel-induced waves. Other studies extended our knowledge on hydrodynamic forcing parameters in estuaries and their impact on sediment dynamics such as turbidity maximum dynamics (Uncles et al., 1998; Brenon and Le Hir, 1999; Uncles et al., 2002; Dyer et al., 2004) and mudflat dynamics (Dyer et al., 2000; Le Hir et al., 2000). Whatever the system studied, estuarine sediments entail a variety of mechanisms in a complex cycle (Eisma, 1993): erosion, resuspension, flocculation, settling, deposition, consolidation. Erosion and resuspension of bed sediments occur when the bottom shear stress reaches critical values (Mitchener and Torfs, 1996; Black, 1998). This threshold value is described in the literature as a function of bed sediment properties such as mud/sand composition, compaction, bed roughness length and biological benthic activity (Mitchener and Torfs, 1996; Maa et al., 1998; Tolhurst et al., 2000; Droppo et al., 2001; Sanford and Maa, 2001). Once the shear stress exceeds a critical value, bed sediments are eroded and resuspended in the water column and are therefore subjected to flocculation processes and horizontal transport. Similarly to erosion and resuspension processes, flocculation processes - described as the aggregation and fragmentation of cohesive particles (van Leussen, 1994; Eisma, 1996) - are driven by sediment properties and biological activity but predominantly by the turbulence variability (Manning and Dyer, 1999; Mikes, et al., 2004). In our case, suspended particles are eventually transported out of the system by the river flow and tidal flow or settle, depending on particle characteristics such as size and density (Dyer, 1994; Manning and Dyer, 1999) and turbulence in the water column.

All these studies revealed the key role played by hydrodynamic forcing parameters on sediment transport processes in estuaries. Moreover, according to the morphological conceptual model described by Dalrymple et al. (1992), hydrodynamic forcing and the resulting intensity of shear stress vary in a macrotidal estuary between the mouth and the tidal limit. This conceptual model proposes dividing up an estuary according to the morphological and hydrodynamic features of each section. In the case of macrotidal estuaries, the model proposes dividing the estuary into three compartments: a river dominated one, an intermediate – mixed energy one and a marine dominated one.

Previous studies on in situ turbulence measurements in estuaries focused on single point measurements, mainly on mudflats at the mouth or near the turbidity maximum zone (Fugate and Friedrichs, 2002; Nikora et al., 2002; Dyer et al., 2004). These studies examined the influence of hydrodynamic forcing parameters on local sediment dynamics, but did not explain the spatial variability of the bottom shear stress within an estuary and particularly its impact on dynamics in areas where fine sediments accumulate. The purpose of this study was to make high-frequency near-bed turbulence measurements on fine sedimentation areas representative of the different morphodynamic and hydrodynamic parts of the macrotidal Seine estuary during low water discharge and during both neap and spring conditions. The objective of the study was to investigate tidally-induced shear stress variations in the Seine estuary and to provide shear stress ranges for each estuarine compartment of the conceptual model.

FIELD SITE

The Seine estuary is a meandering system subjected to a macrotidal regime (Fig. 1). The estuary is hyposynchronous with a double high tide during spring tide conditions (tidal range of 8m) and synchronous during neap tide conditions (tidal range of 4m) (Guezennec, 1999; Guezennec et al., 1999). The tidal range decreases from 8m at the mouth to 2.5m at the tidal limit during spring tides. The tidal propagation is stopped 160km upstream from the mouth by the Poses lock and low tidal reflection was observed. Study sites in the estuary were determined using the kilometric point (kp) location system established for French estuaries. The reference position kp0 is Pont Marie, (Paris), and the upstream limit of the Seine estuary is located at kp202 (Fig. 1).

Guezennec (1999) identified three compartments in the Seine estuary by considering salt intrusion into the estuary (Fig. 1): the upstream compartment corresponds to the tide-affected fluvial fresh water zone, which is limited upstream by the tidal limit and downstream by the salt intrusion limit located near Caudebec en Caux 70km from the mouth (kp310); the mid compartment corresponds to the an area with a high salinity gradient where a turbidity maximum is observed during low water discharge periods (Avoine, 1981; Guezennec et al., 1999; Le Hir et al., 2001); the marine compartment is limited to the estuary mouth, and corresponds to low salinity gradient area. In addition, observations from Guezennec (1999) regarding water levels at low tide in neap and spring conditions identified the presence of a characteristic point near Le Trait (kp308) where low tide water levels are constant over a semi lunar cycle (Fig. 1).

Few current velocity measurements have been undertaken in the Seine estuary: specific areas were studied near Rouen and at the estuary mouth, mainly in the main navigation channel (Data from the Port of Rouen Authorities in Guezennec (1999)). This primary dataset was supplemented by results from validated numerical models (Brenon and Le Hir, 1999). These results revealed longitudinal variations in flood/ebb currents as tides propagate into the estuary (Fig. 1) (Brenon, 1997). During spring tide and low water discharge conditions, the current velocity in the main channel is characterized by a strong flood current for a short period in the mouth (2m s^{-1} current velocity for a one-hour period), a four-hour period with flood current velocities below 0.5m s^{-1} and a long constant ebb current velocity period with current speed of 1m s^{-1}. These maximal flood and ebb current velocities in the main channel as well as the flood/ebb current ratio first increase in the middle estuary (flood current velocity of 2.5m s^{-1}) and then decrease upstream, with 1m s^{-1} flood current velocity at the water surface measured near Le Trait [B] (Fig. 1) and 0.5m s^{-1} in Rouen 20 km downstream from Oissel [A] (Guezennec, 1999).

Current velocities were not homogenously distributed in cross sections due to the meandering morphology. Guezennec (1999) measured surface current velocity in the inner and outer parts of a meander in the Seine estuary 20km downstream from Rouen. This author showed that maximum flood (respectively maximum ebb) current velocity in the outer part was 50% higher than in the inner part (30%). The maximum flood current velocity decreased from 1.0m s^{-1} in the outer part to 0.6m s^{-1} in the inner part, and maximum ebb currents decreased from 1.0m s^{-1} to 0.7m s^{-1}. As a result, these lower hydrodynamic intensity zones are preferential areas for deposition of fine sediments.

In order to determine variability of shear stress intensity from the upstream tidal limit to the estuary mouth, stations typical of mudflats of these areas were chosen as sites for hydrodynamic measurements (Fig. 1). These stations are listed in order from the fluvial to the marine part of the estuary. The Oissel mudflat [A; kp230] is a typical fine sediment storage area for the undredged fluvial part of the estuary (Guezennec et al., 1999; Deloffre et al., 2005). Le Trait mudflat [B; kp300] is located downstream from Rouen, where the fluvial estuary is embanked and dredged, and near the characteristic point discussed by Guezennec et al. (1999). Petiville mudflat [C; kp325] is located in the turbidity maximum zone during low water discharge and is representative of the middle estuary. Stations [A], [B] and [C] are located in the centre of the mudflat away from large natural or human structures that could perturb the river flow. These stations are located 2m above the low water tide level, so they are subjected to comparable flood and ebb durations. They are not influenced by wind, but wave events caused by barges and sea vessels navigation occur intermittently. The Vasière nord [D; kp355] is the largest mudflat of the Seine estuary and is located at its mouth (Lesourd et al., 2003). This site differs from the others as it is separated from the main channel by a submersible dyke, and is crossed by large runnels; it is located 6m above the low water tide level, and is consequently only flooded during slack water periods. The flood and ebb periods are thus shorter and tidal currents are assumed to be lower than those observed at the other stations. However, this mudflat was chosen because of its importance in terms of sediment storage capacity. Station [D] is mainly controlled by wind waves and swell (Lesourd et al., 2003; Deloffre et al., in press).

Measurements were made during successive tidal cycles at stations [A], [B] and [C] during the 03/05/2004 to 13/05/2004 period, i.e. during spring and neap conditions. Spring tide corresponds to tidal amplitudes over 7.5m at the mouth and neap tide to tidal amplitudes below 6.8m. Spring and neap tide surveys were carried at station [D] on the 21/03/2003 and on the 31/03/2003 respectively. Tidal amplitude for these to surveys was 8.05 and 7.5 m respectively. Due to the altitude of station [D], the water height above the mudflat did not exceed 0.5 m for lower tidal range, which is the operational height limit for ADV measurements. Throughout the surveys, river water discharge was lower than 400 $m^3 s^{-1}$ which is the mean annual water discharge of the Seine River.

MATERIAL AND METHODS

Methods used for measurement of current and calculation of turbulence

The recent development of new acoustic Doppler devices such as ADCPs and ADVs enables high frequency and high accuracy 3D current velocity measurements and consequently good quality measurement of turbulence (Kawanisi and Yokosi, 1997; Fugate and Friedrichs, 2002; Nikora et al., 2002; Voulgaris and Meyers, 2004; Simpson et al., 2005).

All stations were instrumented with a 6 MHz Nortek Vector Acoustic Doppler Velocimeter. Shear stress intensities in the water column reach the highest values close to sediment/water interface (Simpson et al., 2005). Higher in the water column, the turbulent energy is partially dissipated and its intensity decreases. The ADV was consequently set up for near-bed measurements with the 0.8cm^3 sampling cell located 7cm above the bed. The apparatus was fixed on a rigid aluminium frame, directed perpendicularly towards the main channel axis to minimize frame-induced noise. This set-up is particularly suitable for shear stress measurements as discussed in various studies (Kawanisi and Yokosi, 1997; Kim et al., 2000; Nikora, et al., 2002; Voulgaris and Meyers, 2004). Velocity measurements were recorded in the East/North/Up coordinates, automatically compensating for possible movement of the instrument using data provided by the ADV internal compass. This minimizes errors due to ADV misalignment with the vertical. Next, the horizontal East/North coordinates were changed to the streamward/crossward reference coordinates, u is then the alongshore velocity and v the cross-shore velocity.

ADV enables measurement of the three components of current velocity with an accuracy of 0.5% of the measured velocity, 7 cm above the bed. Each component of the instantaneous velocity u, v, w can be separated into an averaged part $\overline{U}, \overline{V}, \overline{W}$ and a fluctuating part u’, v’, w’, such as: $u = \overline{U} + u'$ (respectively v and w). The average time step was set to 1 min for calculations. The three mathematical formulations most used in the literature are described below.

The near-bed logarithmic profile method (LP)

Classical tank turbulence measurements are based on the logarithmic velocity profile method (LP), which uses the von Karman – Prandtl equation to estimate the friction velocity u*:

(1) $$\frac{U(z)}{u*} = \frac{1}{\kappa} \log\left(\frac{z}{z_0}\right)$$

where U(z) is the mean current velocity at height z above bed, κ is the Von Karman constant and z_0 is the bed roughness length. This method requires velocity measurements at various heights in the water column to reproduce and fit the current velocity log-profile (Fugate and Friedrichs, 2002). For studies requiring single point measurements, as was the case in the present study, correct estimation of the bed roughness value is needed. However, recent studies revealed the complexity involved in estimating roughness value, with measurements ranging from 0.1 to 1mm for muddy sediment (Voulgaris and Meyers, 2004). Soulsby (1997) proposed values ranging from 0.2mm for muddy sediments to 0.7mm for mud/sand sediment. The Seine intertidal mudflats concerned here are mainly made of mud, and a bed roughness value of 0.2 mm was thus used. To compare methods used to calculate shear stress values, the friction velocity u* calculated from the logarithmic method was transformed to the bottom shear stress τ_{LP} value by applying:

(2) $$\tau_{LP} = \rho u*^2$$

The Covariance method (COV)

Calculating the total shear stress requires both the Reynolds shear stress (τ_{Re}) and the viscous stress ($\tau_{VISCOUS}$) (Stacey et al., 1999). Nikora et al., 2002 estimated $\tau_{VISCOUS}$ using the linear relationship expressing viscous stress as a function of the time-averaged current velocity and the distance z up to the bed:

$$(3) \qquad \tau_{viscous} = \rho\,\nu\,\frac{\overline{du}}{dz} \cong \rho\,\nu\,\frac{|U(z)|}{z}$$

τ_{Re} was estimated using the classical relationship involving the two Reynolds components:

$$(4) \qquad \tau_{Re} = -\rho\left(\overline{u'w'} + \overline{v'w'}\right)$$

(Soulsby, 1983; Dyer et al., 2004; Voulgaris and Meyers, 2004). Thus, total shear stress (τ_{COV}) is estimated as: $\tau_{COV} = \tau_{Re} + \tau_{viscous}$.

The Turbulent Kinetic Energy method (TKE)

The TKE method expresses the TKE shear stress (τ_{TKE}) proportionally to the turbulent kinetic energy K:

$$(5) \qquad K = \frac{1}{2}\left(\overline{u'^2} + \overline{v'^2} + \overline{w'^2}\right)$$

$$(6) \qquad \tau_{TKE} = \rho\,C_{TKE}\,K$$

C_{TKE} coefficient values ranging from 0.19 to 0.21 are commonly cited in the literature for near-bed measurements (Soulsby, 1983; Kim et al., 2000). In our study, all measurements were made at the same height above the bottom, i.e. 7cm above the bed, and an average constant value of 0.2 was used for the calculation of τ_{TKE}.

A typical dataset recorded at Le Trait mudflat during neap tide is presented in Fig. 2 to compare the mathematical formulations used to calculate shear stress values. This comparison reveals that the three methods are well correlated. The LP shear stress values exceed τ_{COV} values during high current velocity periods for both flood and ebb periods (Fig. 2). This could be due to the variability of the surface sediment properties, i.e. bed roughness length.

Discrepancies at Le Trait mudflat were observed during short events with high shear stress values ($\tau_{TKE} > 1 Nm^{-2}$). These events were caused by waves generated by barges or sea vessels sailing the Seine estuary. The LP method is not sensitive to waves as it is based on mean current velocity measurements. In contrast, the TKE method is highly influenced by waves because orbital velocities increase fluctuations in velocity (Soulsby and Humphery, 1990).

However, effects of wave events are beyond the scope of this study and will not be discussed further in this paper. Our interpretation and discussion of the results only focuses on periods not affected by wind waves or boat-induced waves, where the three methods are equivalent. τ_{COV} is thus used to represent shear stress values thereby clarifying our results.

Sediment features

Sediment bulk density and grain-size distribution of each mudflat were measured during each tidal survey. Bed sediments were collected just after mudflat emersion and measurements were made in the laboratory. Grain-size distributions were obtained with a Beckman laser Coulter LS 230 measuring a size-spectrum from 0.04 to 2000µm. Bulk density was obtained from water content measurements (W%):

(7) $$\rho_b = \rho + \left(\frac{\rho_S - \rho}{\rho_S}\right)\left(\frac{\rho}{\frac{W\%}{100} + \frac{\rho}{\rho_S}}\right)$$

where W% is the ratio between the water mass and the dry sediment mass.

RESULTS

Neap tide

Figures 3a and 3b present the general hydrological conditions on the mudflats studied along the Seine estuary in neap tide conditions. The water height zero reference was set locally at the low slack water level for each site. The tidal range during neap tide is 6m at the mouth, decreases upstream to 4m at station [C], and reaches 2m close to the dynamic tidal limit [A]. Maximum water height at the “Vasière Nord” [D] did not exceed 1.5m due to the altitude of the mudflat. Similarly to the water height, the maximum current velocity measured above the intertidal mudflats decreases from the mouth to the fluvial part of the estuary from 0.5m s^{-1} to 0.2m s^{-1} respectively.

The first station located in the upstream fluvial part was ebb dominated. The flood period in station [A] was short and of low intensity with current velocity values lower than 0.2m s^{-1}. Flood/ebb current reversal occurred two hours before high water, and ebb currents slowly rose to reach a maximum value of 0.2m s^{-1}.
The hydrodynamics at station [B] was flood/ebb balanced, with symmetrical behaviour before and after high water. The maximum current velocity was 0.25m s^{-1} at the beginning of the flood period and at the end of the ebb period, and current velocity inversion occurred during the high slack water period.
Station [C] and [D] were flood dominated. Flood currents at station [C] rapidly reached the maximum values of 0.4m s^{-1} half an hour after mudflat immersion, and decreased slightly until flood/ebb current reversal two hours after high water. Ebb currents increased rapidly to reach a mean velocity value of 0.3m s^{-1}. Station [D] is located on the “Vasière Nord” mudflat, 4m higher than the other stations and despite the large tidal range at the estuary mouth, only the end

of the flood period, slack water and the onset of the ebb period were recorded, i.e. the periods of lower energy during a tidal cycle. The mudflat was characterized by low water height (below 60cm) and low current velocities (below 0.2m s^{-1}) in neap tide conditions.

Spring tide

During the spring tide conditions, a tidal range of 8m was observed at the estuary mouth, this range decreased slightly to reach 3m at station [A] close to the tidal limit (Fig. 4a). The tidal wave propagates into the estuary with a pronounced asymmetric shape that increases from the estuary mouth to the upstream boundary. A double high water slack was observed at stations [C] and [D]. The hydrodynamic features in spring tide conditions were similar to those observed during neap tides at the downstream stations [B], [C] and [D], with higher current velocities up to 1m s^{-1} at station [C] (Figure 4b). However, differences were observed at station [A] where the current reversal period corresponded to the high slack water period and flood and ebb periods followed a similar pattern with maximum current speed of 0.2m s^{-1} and equal ebb/flood periods.

Shear stress measurements

Shear stress variations for neap and spring tides conditions are presented in Fig. 3c and 4c. τ_{COV} decreased from the estuary mouth to the fluvial part, with maximum values of 0.8N m^{-2}, 0.15N m^{-2} and 0.05N m^{-2} for stations [C], [B] and [A] during neap tide conditions and 1N m^{-2}, 0.4N m^{-2} and 0.2N m^{-2} during spring tide conditions respectively.

Shear stress variations during a tidal cycle for both neap and spring tides were similar for stations [B] and [C]. Large shear stress values were observed on mudflats during flood and ebb periods, and values - less than 0.01N m^{-2} - were observed during high slack water periods. The occurrence of the maximum shear stress value above the intertidal mudflats during the tidal cycle depends on the location of the station in the estuary and on the moment in time in the semi lunar cycle. The highest τ_{COV} were observed during flood periods in both neap and spring tide conditions at station [C] (τ_{COV} values of 0.8 and 1N m^{-2} respectively) and during spring tide conditions at station [B] (τ_{COV} values of 0.4N m^{-2}). Shear stress values during neap tides at station [B] were similar for both flood and ebb periods, with a τ_{COV} value of 0.15N m^{-2}. During neap tides, τ_{COV} values below 0.05N m^{-2} were measured at station [A]. During spring tide conditions, τ_{COV} reached values exceeding 0.1N m^{-2} during the flood period, the high slack water period and the ebb period.

Due to the higher altitude of the mudflat, station [D] was never subjected to the most energetic flood and ebb conditions and thus did not display noticeable shear stress during neap and spring tides. However, the "Vasière Nord" mudflat experienced τ_{COV} values that were consistently greater than 0.05N m^{-2} while current velocity values were less than 0.1m s^{-1}. These shear stress values can be attributed to period of wind or waves of small amplitude (<0.05m) but which nevertheless had a marked influence on the bottom shear stress due to the low water height (<0.6m).

DISCUSSION

Comparative methods for calculation of shear stress

According to Kim et al. (2000), TKE, COV and LP methods present similar values (Fig. 2). The combined use of these three methods of calculation can be a useful way to evaluate the individual effects of the parameters that control turbulent processes, i.e. tidal currents and waves. The LP method, which is based on mean current velocities, is useful to determine tidally-induced shear stress because high frequency variations are integrated in the time averaging operation. The LP method is optimal when current velocity profiles are recorded as it allows both accurate calculations of bed roughness length and shear stress values. This method can also be used when current velocity profiles are not available but in this case requires a priori estimation of the bed roughness length value. This estimation generates serious errors in the friction velocity calculations (Fig. 2). TKE and COV methods operate from similar inputs, i.e. the fluctuating part of the current velocity. However, with the TKE method, shear stress values are calculated from the turbulent kinetic energy K by using (6). τ_{TKE} then depends on the choice of the C_{TKE} , which ranges from 0.19 (Soulsby, 1983; Dyer et al., 2004) to 0.21 (Kim et al., 2000). With tidal flows, COV and TKE methods are theoretically equivalent, and τ_{COV} and τ_{TKE} can be compared as:

(8) $$\tau_{COV} = \tau_{TKE} = \rho\, C_{TKE}\, K$$

The comparison of the combined results of spring and neap surveys is presented in Fig. 5; a linear regression was used to estimate C_{TKE}. Values were well correlated (R>0.95) with the best fit C_{TKE} value of 0.19 (Fig. 5), in agreement with the value proposed by Soulsby (1983).

Relationships between tidal currents and friction velocity

Correlations between observations of current velocity and turbulence shear stress measurements are obvious if both friction velocities calculated from the τ_{COV} and the time-averaged current velocities are plotted, after truncating the wave events (Fig. 6). Considering the flow as fully turbulent, the friction velocity u* is calculated as a function of the local shear stress at the height z and empirically corrected from the water height variations:

$$u^* = \sqrt{\frac{\tau_{COV}}{\rho.\left(1 - \frac{z}{h}\right)}} \quad (9)$$

(Voulgaris and Trowbridge, 1998; Stacey et al., 1999; Voulgaris and Meyers, 2004).

Linear regression fits are based on the following formulation: $u^* = \alpha\, U + \beta$. The constant in the regression line is always smaller than 0.001, which validates the logarithmic form of the flow and data consistency (Collins et al., 1998). Flood and ebb components are fitted separately (α_F and α_E correspond respectively to flood and ebb periods) in order to examine possible changes in the bed sediment properties with respect to flood and ebb periods as found by Collins et al. (1998) and Voulgaris and Meyers (2004). These coefficients are related to the drag coefficient values measured close to the bed by applying the formulation: $C_d = \alpha^2$. Calculating best-fit linear relationships between current velocity and friction velocities is equivalent to estimating the bed roughness by applying the LP method used for turbulent intensity calculations (Eq. 1). This equation can be transformed to express u* as a function of the mean value of the time series of current velocity values U(z), and thus becomes (Collins et al., 1998):

$$u^* = \frac{\kappa}{\ln\left(\frac{z}{z_0}\right)} U \quad (10)$$

Therefore the best-fit regression coefficient α is related to the bed roughness value, assuming that the sampling height z is known (in the present study, z=7cm) (Table I). In this study, the bed roughness is considered to be only skin roughness and is associated with sediment grain-size characteristics. In our study, topographic variations in bedform that also contribute to the bed roughness length were not considered, as the deployment station was located in the flattest area of the mudflats far from runnels and channels.

Current velocities and friction velocities values are well correlated (Figure 6 – Table I), and a consistent feature was observed at the three stations with higher best-fit constant values during flood periods, and therefore higher drag coefficient and bed roughness values: the bed roughness length decreased from 0.34mm during the flood stage to 0.18mm during the ebb stage at station [A] and from 0.03 to 0.01mm at stations [B] and [C]. These observations could be due to a change in sediment properties during the tidal cycle, which, in turn, could be due to finer grained sediment or biological activity (Voulgaris and Meyers, 2004). Averaged bed roughness length values were calculated to 0.02 mm for stations [B] and [C] and 0.26mm for station [A]. These variations in length could be due to specific sediment properties at stations [A], [B] and [C]. Bed roughness length values were then compared with bed sediment features (Table II). Bed sediments at stations [B] and [C] were mostly muddy, and the calculated bed roughness length values are close to the median value (30µm) of the sediment particle size distribution (Table II). Nevertheless, the bed roughness length value at station [A] is three times higher than the median size of 77µm. Sediment at station [A] is a mixture of sand and mud, with mode values of 120µm and 20µm respectively. Mitchener and Torfs (1996) showed that values for bed roughness length are high for mixed bed sediments, which could explain the high bed roughness length values found here. These results are in agreement with the recent work of Voulgaris and Meyers (2004) who estimated bed roughness length values ranging from 0.026mm to 0.1mm for silt sediments with an occasional sand fraction. However, they are lower than those proposed by Soulsby (1997) i.e. 0.2mm for mud and 0.7mm for a sand/mud mixture.

Unlike the Nikuradse formula that gives the bed roughness length as 1/12.5 fold the median size of sand grains, the linear relationship between particle-size distribution and bed roughness length for muddy or sand/mud sediments for mudflats with no topographic effect is:

$z_0 \approx D_{50}$ for muddy sediments

$z_0 \approx 3\, D_{50}$ for mud/sand mixtures

The 0.2mm bed roughness length value was initially chosen to determine shear stress values by the LP method, which explains the fact that LP shear stress values exceed the τ_{COV} ones during maximal ebb and flood current velocities. The use of a single constant value for bed roughness length during tidal cycles introduces uncertainty in the estimation of bed shear stress. To give an example, for a water current velocity of 0.5m s^{-1}, a change in the bed roughness value from 0.34 to 0.18mm, as observed at station [A], causes a reduction in bottom shear stress from 1.41 to 1.12N m^{-2}. This generates an error of 20% in the estimation of τ_{LP}. Thus careful use of the bed roughness length is required in estuarine systems studies where successive periods of sedimentation and erosion induce a continuous change in the nature of sediment.

Effect of tidally-induced turbulence on sediment dynamics

Based on the present set of data, the near-bed tidally-induced shear stress can be calculated along the macrotidal Seine estuary. Variations in shear stress have a powerful influence on estuarine processes and typical sediment dynamics by controlling bank erosion, sediment resuspension and deposition. Recent studies reported the development of many in situ devices (Tolhurst et al., 2000) or laboratory devices (Mitchener and Torfs, 1996) to measure critical erosion shear stress (τ_{ce}). Field and laboratory experiments on various mixed-sediment samples provided a large dataset that can be used to propose a simple empirical relationship between sediment properties and erosion critical shear stress values. No τ_{ce} measurements were made during the present study, and consequently τ_{ce} estimations were made using different empirical relationships given in the literature linking τ_{ce} and bed bulk density ρ_b:

Mitchener and Torfs (1996) proposed calculating τ_{ce} as a power function of ρ_b

(11) $$\tau_{ce} = E_1(\rho_b - 1000)^{E_2}$$

with E_1 = 0.015 and E_2=0.73. This formulation has been validated for artificially sand/mud mixed sediment with bulk density values ranging from 1000 to 1800kg m^{-3}. However, the results obtained from natural undisturbed sediment with properties close to those observed on the mudflats studied here were one order of magnitude lower than the artificial sediments, and varied with the mud/sand ratio. To give an example, τ_{ce} measured for sediments similar to those in the present study with bulk density values varying from 1200 to 1400kg m^{-3} range from 0.05 to 0.7N.m^{-2} for muddy sediment containing respectively 0% and 20% of sand, and the associated calculated τ_{ce} is of 0.95N m^{-2} (ρ_b~1300kg.m^{-3}). The given relationship thus overestimates critical erosion shear stress values.

Mehta (1988) found the critical erosion shear stress to be a function of the bulk density ρ_b and a ξ -coefficient:

(12) $$\tau_{ce} = \xi\left(\frac{\rho_b - 1000}{1000}\right)$$

ξ is generally estimated to be 1 for cohesive sediments, but this coefficient may be one order of magnitude higher with a sediment with 18% sand content. The calculated τ_{ce} is thus 0.3N m^{-2} for a bulk density value of 1300kg m^3. These τ_{ce} values are close to those measured by Tolhurst et al. (2000) on similar sediments. These two relationships can be used to estimate τ_{ce} values. Nevertheless, all the controlling parameters such as grain size distribution and benthic biological activity, which are known to stabilize bed sediments (Mitchener and Torfs, 1996; Riethmuller et al., 2000; Tolhurst et al., 2000; Droppo et al., 2001) are not taken into account.

Table II summarizes bed sediment features and a range of values of τ_{ce} values calculated with the two methods presented above for the four mudflats investigated in the Seine estuary. Seine mudflat sediments are mixed mud and sand with a higher sand content (>25%) and a higher bulk density (1420kg m^{-3}) at the upstream station [A]. Consequently bed sediment at station [A] is the most stabilized, with τ_{Ce} values ranging from 0.4 to 1.2N m^{-2}. Two critical erosion shear stress intervals are given for the “Vasière Nord” station because a deposition period occurred between the spring and neap surveys. Surface sediment properties consequently varied during these periods and τ_{ce} values ranged from 0.36 to 1.1N m^{-2} and from 0.24 to 0.8N m^{-2}

respectively before and after deposition (Table II). These results are close to the rheological values obtained by Lesourd (2000) on mud samples collected at the mouth of the Seine estuary and used for consolidation experiments. τ_{ce} values estimated by this author ranged from 0.4 to 0.8N m^{-2}, with a rapid increase in τ_{ce} from 30 to 200% one hour after the onset of the experiment. These calculated intervals of critical erosion shear stress were compared with the calculated total shear stress (τ_{COV}) for each site during neap and spring conditions. This comparison reveals that the tidally-induced shear stress never exceeds the critical erosion shear stress values at stations [A] and [D], whatever the spring or neap conditions. At station [B] and only during the early flood stage on spring tide, τ_{COV} values are higher than the lowest calculated τ_{ce} values. Only station [C] is seen to be controlled by the tidal currents, mostly during the flood period and whatever the hydrodynamics conditions. These results provide a first approach to understanding how tidal currents control the process of mudflat erosion. However, these results are based on simple calculations where τ_{ce} is only a function of the bulk density. Moreover, the ADV is operational as soon as sensors are flooded, when the water height above the mudflat exceeds 20cm. Thus it is not possible to make measurements at the critical periods of flood and ebb, when the water just starts to come in and to go out. This means that maximal shear stress values could be underestimated. Both shear stress and τ_{ce} field measurements are now required to confirm the role played by tidal flows in estuarine mudflat dynamics.

Hydrodynamic compartments within the macrotidal Seine estuary

The results obtained in this study are in good agreement with turbulence measurements recently made in macrotidal estuarine systems (Kawanisi and Yokosi, 1997; Dyer et al., 2004; Voulgaris and Meyers, 2004). However some of these sampling stations were located in channels where shear stress values are the highest, while in this present study, the instruments were positioned on several intertidal mudflats. Most of these authors' experiments were carried at a single point in an estuary cross section, and so cannot describe the spatial variability of the hydrodynamic features.

Our results provide support for dividing the Seine estuary into three specific compartments according to the conceptual model proposed by Dalrymple et al. (1992) for meandering tide-dominated estuaries which we modified to consider only intertidal environments (Fig. 7). Two main compartments can be proposed: the first compartment (I) is limited upstream by the dynamic tidal limit and downstream at the characteristic point located near station [B]; this compartment is ebb-dominated with averaged calculated shear stress values lower than 0.3N m^{-2} that do not allow sediment resuspension. The second compartment (II) is limited upstream at the characteristic point and downward downstream at the marine limit of the estuary; this compartment is flood dominated and the tidally-induced shear stress reach values of 1N m^{-2} close to the τ_{ce}. However, intertidal mudflats at the estuary mouth are located 6m above the low water level, and consequently do not present comparable shear stress values: the “Vasière Nord” experiences low tidal current velocities and thus low tidally-induced shear stress values (<0.1N m^{-2}). Previous works carried out at the mouth of the estuary led to a proposal for a third compartment in this area, related to intertidal mudflats, where wind effects are predominant (Silva Jacinto, 2002; Lesourd et al., 2003; Deloffre et al., in press).

AKNOWLEDGMENTS

Funding for this study was partly provided by the European INTERREG III RIMEW program and the Seine Aval Program. Three anonymous reviewers are acknowledged for their helpful comments. We would like to thank Mrs Daphne Goodfellow for her helpful review. Jonathan Taylor and Romaric Verney were funded through two grants provided by the Regional Council of Haute Normandie (France).

LITERATURE CITED

Avoine, J. (1981). Estuaire de la Seine: sédiments et dynamique sédimentaire, Université de Caen, 236p

Black, K.S. (1998). Suspended sediment dynamics and bed erosion in the high shore mudflat region of the Humber Estuary, UK, Marine Pollution Bulletin, 37 (3-7), 122-133

Brenon, I. (1997). Modélisation de la dynamique des sédiments fins dans l'estuaire de Seine, Thèse de 3ème cycle, Université de Bretagne Occidentale, 204p

Brenon, I. and P. Le Hir (1999). Modelling the tubidity maximum in the Seine estuary (France): Identification of formation processes, Estuarine, Coastal and Shelf Science, 49 (4), 525-544

Collins, M.B., X. Ke and S. Gao (1998). Tidally-induced flow structure over intertidal flats, Estuarine, Coastal and Shelf Science, 46 233-250

Dalrymple, R.W., B.A. Zaitlin and R. Boyd (1992). Estuarine facies models: conceptual basis and stratigraphic implications, Journal of Sedimentary Petrology, 62 (6), 1130-1146

Deloffre, J., R. Lafite, P. Lesueur, S. Lesourd, R. Verney and L. Guezennec (2005). Sedimentary processes on an intertidal mudflat in the upper macrotidal Seine estuary, France, Estuarine, Coastal and Shelf Science, 64 (4), 710-720

Deloffre, J., R. Lafite, P. Lesueur, R. Verney, S. Lesourd, A. Cuvilliez and J.A. Taylor (in press). Controlling factors of rhythmic sedimentation processes on an intertidal estuarine mudflat - Role of the maximum turbidity zone in the macrotidal Seine estuary, France, Marine Geology, Droppo, I.G., Y.L. Lau and C. Mitchell (2001). The effect of depositional history on contaminated bed sediment stability, The Science of Total Environment, 266 7-13

Dyer, K.R. (1994). Estuarine Sediment transport and deposition, In: Sediment transport and depositional processes, K. Pye (eds), Blackwell Scientific Publications, Oxford, 193-217

Dyer, K.R., M.C. Christie, N. Feates, M.J. Fennessy, M. Pejrup and W. Van der Lee (2000). An investigation into processes influencing the morphodynamics of an intertidal mudflat, the Dollard Estuary, The Netherlands : I. Hydrodynamics and suspended sediment, Estuarine, Coastal and Shelf Science, 50 (5), 607-625

Dyer, K.R., M.C. Christie and A.J. Manning (2004). The effects of suspended sediment on turbulence within an estuarine turbidity maximum, Estuarine, Coastal and Shelf Science, 59 (2), 237-248

Eisma, D. (1993). Suspended matter in the aquatic environment, Springer-Verlag, 315p

Eisma, D. (1996). Flocculation and defloculation of suspended matter in estuaries, Netherlands Journal of Sea Research, 20 (2/3), 183-199

Fugate, D.C. and C.T. Friedrichs (2002). Determining concentration and fall velocity of estuarine particle populations using ADV, OBS and LISST, Continental Shelf Research, 22 1867-1886

Guezennec, L. (1999). Hydrdynamique et transport en suspension du matériel particulaire fin dans la zone fluviale d'un estuaire macrotidal : l'exemple de l'estuaire de la Seine (France), Thèse de 3ème cycle, Université de Rouen, 240p

Guezennec, L., R. Lafite, J.P. Dupont, R. Meyer and D. Boust (1999). Hydrodynamics of suspended particulate matter in the tidal freshwater zone of a macrotidal estuary (the Seine estuary, France), Estuaries, 22 (3A), 717-727

Kawanisi, K. and S. Yokosi (1997). Characteristics of suspended sediment and turbulence in a tidal boundary layer, Continental Shelf Research, 17 (8), 859-875

Kim, S.-C., C.T. Friedrichs, J.P.-Y. Maa and L.D. Wright (2000). Estimating bottom stress in tidal boundary layer from acoustic doppler velocimeter data, Journal of Hydraulic Engineering, 126 (6), 399-406

Le Hir, P., A. Ficht, R. Silva Jacinto, P. Lesueur, J.-P. Dupont, R. Lafite, I. Brenon, B. Thouvenin and P. Cugier (2001). Fine sediment transport and accumulations at the mouth of the Seine Estuary (France), Estuaries, 24 (6B), 950-963

Le Hir, P., W. Roberts, O. Cazaillet, M.C. Christie, P. Bassoullet and C. Bacher (2000). Characterization of intertidal flat hydrodynamics, Continental Shelf Research, 20 1433-1459

Lesourd, S. (2000). Processus d'envasement d'un estuaire macrotidal: zoom temporel du siècle à l'heure; application à l'estuaire de la Seine, Thèse de 3ème cycle, Université de Caen, 290p

Lesourd, S., P. Lesueur, J.C. Brun-Cottan, S. Garnaud and N. Poupinet (2003). Seasonal variations in the characteristics of superficial sediments in a macrotidal estuary (the Seine inlet, France), Estuarine, Coastal and Shelf Science, 58 (1), 3-16

Maa, J.P.-Y., L. Sanford and J. Halka (1998). Sediment resuspension characteristics in Baltimore Harbour, Maryland, Marine Geology, 146 137-145

Manning, A.J. and K.R. Dyer (1999). A laboratory examination of floc characteristics with regard to turbulent shearing, Marine Geology, 160 147-170

Mehta, A.J. (1988). Laboratory studies on cohesive sediment deposition and erosion, In: Physical processes in estuaries, Dronkers and W. van Leussen (eds), Springer-Verlag, 427-445

Mikes, D., R. Verney, R. Lafite and M. Belorgey (2004). Controlling factors in estuarine flocculation processes : experimental results with material from the Seine Estuary, Northwestern France, Journal of coastal research, 41 82-89

Mitchener, H. and H. Torfs (1996). Erosion of mud/sand mixtures, Coastal Engineering, 29 1-25

Nikora, V., D.G. Goring and A. Ross (2002). The structure and dynamics of the thin near-bed layer in a complex marine environment: a case study in Beatrix Bay, New Zealand, Estuarine, Coastal and Shelf Science, 54 915-926

Riethmuller, R., M. Heineke, H. Kuhl and R. Keuker-Rugiger (2000). Chlorophyll a concentration as an index of sediment surface stabilisation by macrophytobenthos?, Continental Shelf Research, 20 1351-1372

Sanford, L.P. and J.P.-Y. Maa (2001). A unified erosion formulation for fine sediments, Marine Geology, 179 9-23

Silva Jacinto, R. (2002). Action des vagues sur les estrans et vasières. Application à l'estuaire de Seine, Thèse de 3ème cycle, Université de Rouen, 231pp

Simpson, J.H., E. Williams, L.H. Brasseur and J.M. Brubaker (2005). The impact of tidal straining on the cycle of turbulence in a partially stratified estuary, Continental Shelf Research, 25 51-64

Soulsby, R.L. (1983). The bottom boundary layer of shelf seas, In: Physical oceanography of coastal and shelf seas, B. Johns (eds), Elsevier, Amsterdam, 189-266

Soulsby, R.L. (1997). Dynamics of marine sands. A manual for practical applications, (eds), Thomas Telford, London,

Soulsby, R.L. and J.D. Humphery (1990). Field observations of wave-current interaction at the sea bed, In: Water wave kinematics, A. Torum and O. T. Gudmestad (eds), Kluwer Academic Publishers, 413-428

Stacey, M.T., S.G. Monismith and J.R. Burau (1999). Measurements of Reynolds stress profiles in unstratified tidal flow, Journal of Geophysical Research, 104 (C5), 10,933-10,949

Tolhurst, T.J., K.S. Black, D.M. Paterson, H.J. Mitchener, G.R. Termaat and S.A. Shayler (2000). A comparison and measurement standardisation of four in situ devices for determining the erosion shear stress of intertidal sediments, Continental Shelf Research, 20 1397-1418

Tolhurst, T.J., R. Riethmuller and D.M. Paterson (2000). In situ versus laboratory analysis of sediment stability from intertidal mudflats, Continental Shelf Research, 20 1317-1334

Uncles, R.J., A.E. Easton, M.L. Griffiths, C.K. Harris, R.J.M. Howland, R.S. King, A.W. Morris and D.H. Plummer (1998). Seasonality of the turbidity maximum in the Humber-Ouse Estuary, UK, Marine Pollution Bulletin, 37 (3-7), 206-215

Uncles, R.J., J.A. Stephens and R.E. Smith (2002). The dependence of estuarine turbidity on tidal intrusion length, tidal range and residence time, Continental Shelf Research, 22 1835-1856

van Leussen, W. (1994). Estuarine macroflocs : their role in fine grained sediment transport, University of Utrecht, 488pp

Voulgaris, G. and S.T. Meyers (2004). Temporal variability of hydrodynamics, sediment concentration and sediment settling velocity in a tidal creek, Continental Shelf Research, 24 (15), 1659-1683

Voulgaris, G. and J.H. Trowbridge (1998). Evaluation of the acoustic doppler velocimeter (ADV) for turbulence measurements, Journal of Atmospheric and oceanic technology, 15 272-289

	Flood			Ebb		
Site	α_F	Cd (x10^{-3})	z_0 (mm)	α_E	Cd (x10^{-3})	z_0 (mm)
[A]	0,072	5,6	0,34	0,067	4,5	0,18
[B]	0,051	2,6	0,027	0,043	1,8	0,006
[C]	0,051	2,8	0,027	0,046	2,1	0,012

Table I: Summary of drag coefficient (Cd), bed roughness length (z_0) and best-fit constant values α at Oissel [A], Le Trait [B] and Petiville [C] calculated during flood and ebb stages

Station	Site	Bed concentration (g/l)	Bulk density (g/l)	% Silt	% Sand	Critical shear stress (N m^{-2}) *Mitchener and Torfs (1996)*
A	Oissel	678	1422	73.5	26.5	1.24
B	Le Trait	476	1296	82.0	18.0	0.96
C	Petiville	431	1268	84.0	16.0	0.89
D	Vasière Nord (NT)	579	1360			1.10
	Vasière Nord (ST)	389	1242			0.82

Table II: Bed sediment properties at the four intertidal mudflats studied

FIGURE LEGENDS

Fig. 1: The Seine estuary: hydrodynamic feature and sites studied. Main channel current velocity values provided by the Port Autonome de Rouen (From Guezennec, 1999).

Fig. 2: Turbulent shear stress values calculated with three different methods (Turbulent Kinetic Energy (TKE), Logarithmic profile (LP) and Covariance (COV) methods). Case of a tidal survey at Le Trait [B]. The LP shear stress is calculated considering a bed roughness length value of 0.2mm

Fig. 3: Time series of water height (a), current velocity (b) and total shear stress (τ_{COV}) (c) above the four intertidal mudflats in neap tide conditions. A: Oissel; B: Le Trait; C: Petiville; D: Vasière Nord. Solid line (a) symbolizes the flooded periods and the dotted line the water height in the main channel.

Fig. 4: Time series of water height (a), current velocity (b) and total shear stress (τ_{COV}) (c) above the four intertidal mudflats in spring tide conditions. A: Oissel; B: Le Trait; C: Petiville; D: Vasière Nord. Solid line (a) symbolizes the flooded periods and the dotted line the water height in the main channel.

Fig. 5: Relationship between the Turbulent kinetic Energy (K) and the Total shear stress (τ_{COV}) values. The solid line shows the best fit (linear least squares regression analysis) of τ_{COV} values regarding K ones. The constant C_{TKE} =0.19 value is deduced from this linear fit.

Fig. 6: Friction velocity as a function of the mean current velocity: linear relationship fits.

Fig. 7: Maximum tidally-induced shear stress values on intertidal mudflats along the Seine estuary during flood (black dots) and ebb stages (grey dots), during neap and spring tide conditions. The dashed line represents the schematic evolution of the bed shear stress for mudflats located 2m above the low water height. Dark lines symbolizes the flood phase and grey lines the ebb phase.

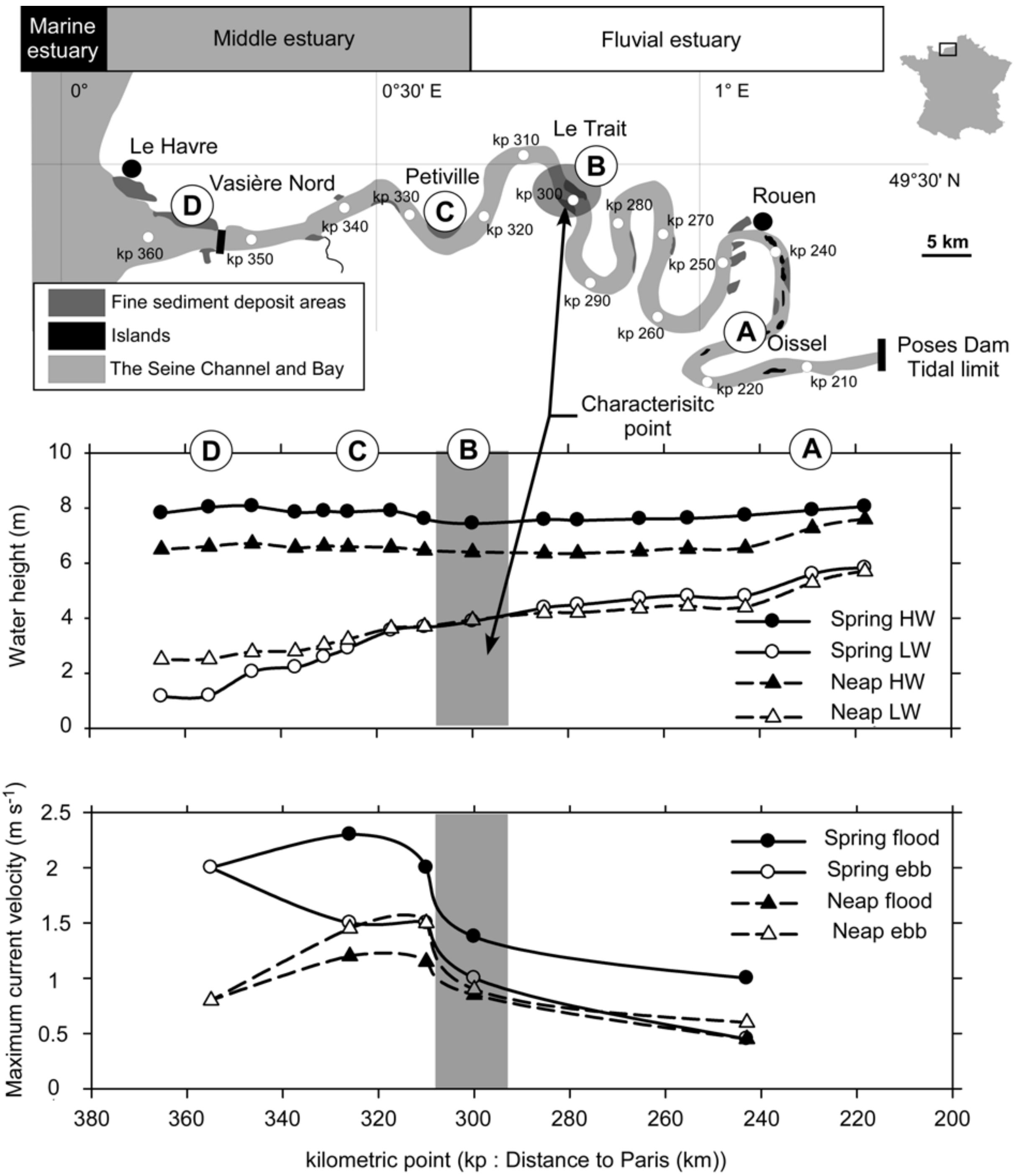

Marine estuary
Middle estuary
Fluvial estuary
0°
0°30' E
1° E
49°30' N
Le Havre
Vasière Nord
Petiville
Le Trait
Rouen
Oissel
Poses Dam
Tidal limit
kp 360
kp 350
kp 340
kp 330
kp 320
kp 310
kp 300
kp 290
kp 280
kp 270
kp 260
kp 250
kp 240
kp 220
kp 210
5 km
Fine sediment deposit areas
Islands
The Seine Channel and Bay
Characterisitc point
Water height (m)
Spring HW
Spring LW
Neap HW
Neap LW
Maximum current velocity (m s-1)
Spring flood
Spring ebb
Neap flood
Neap ebb
kilometric point (kp : Distance to Paris (km))

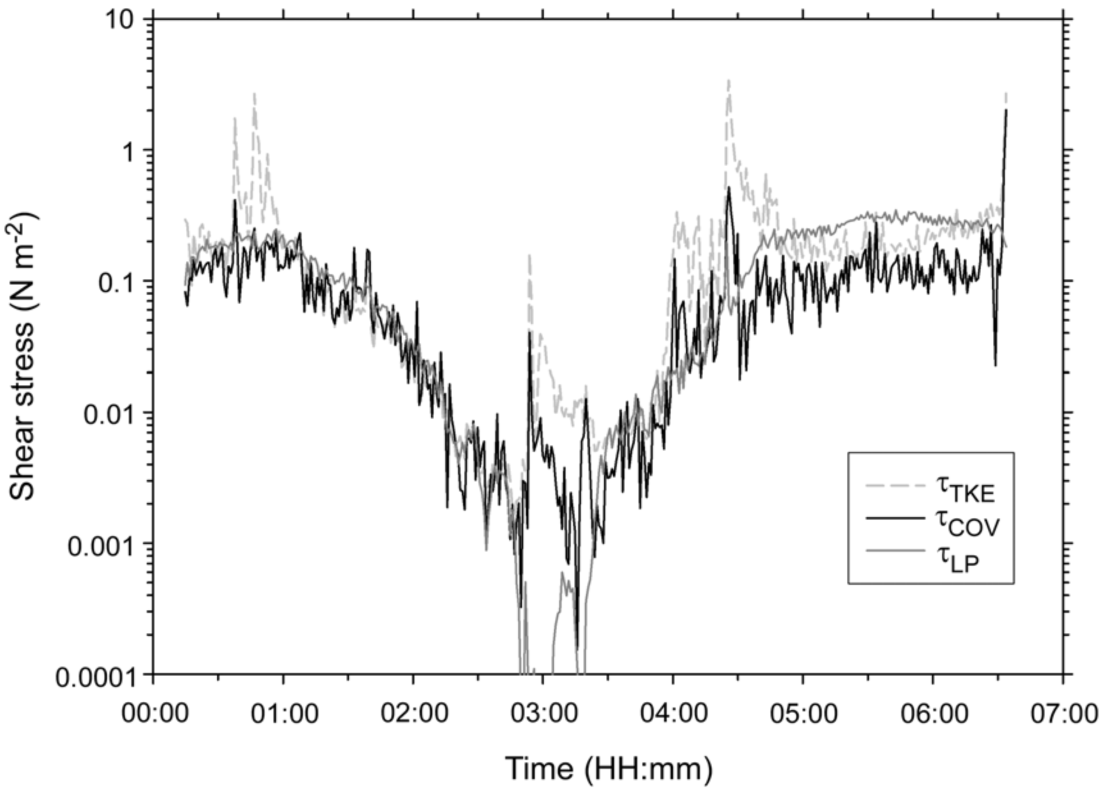

Fig. 2 – Verney et al.

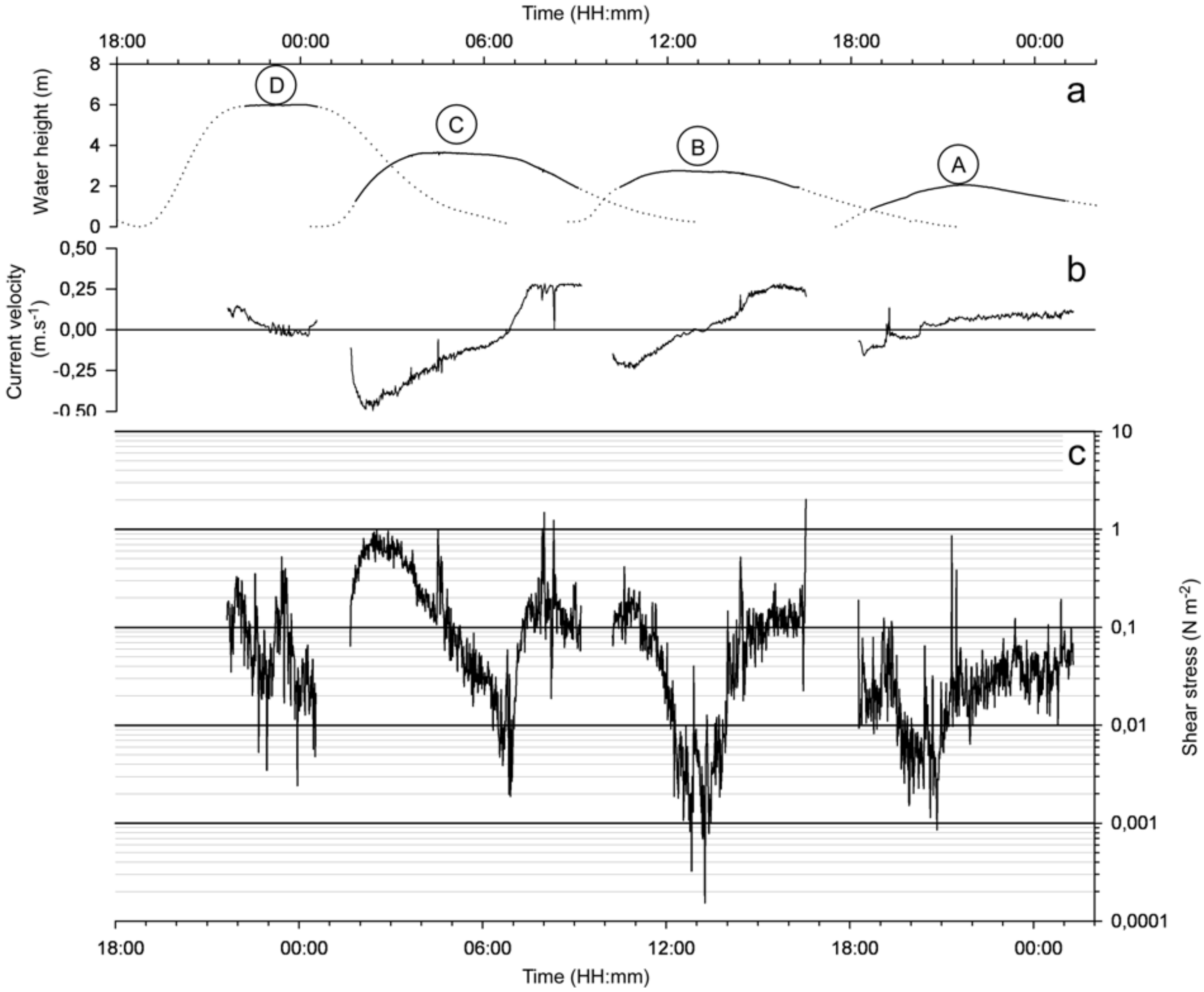

Fig. 3 – Verney et al.

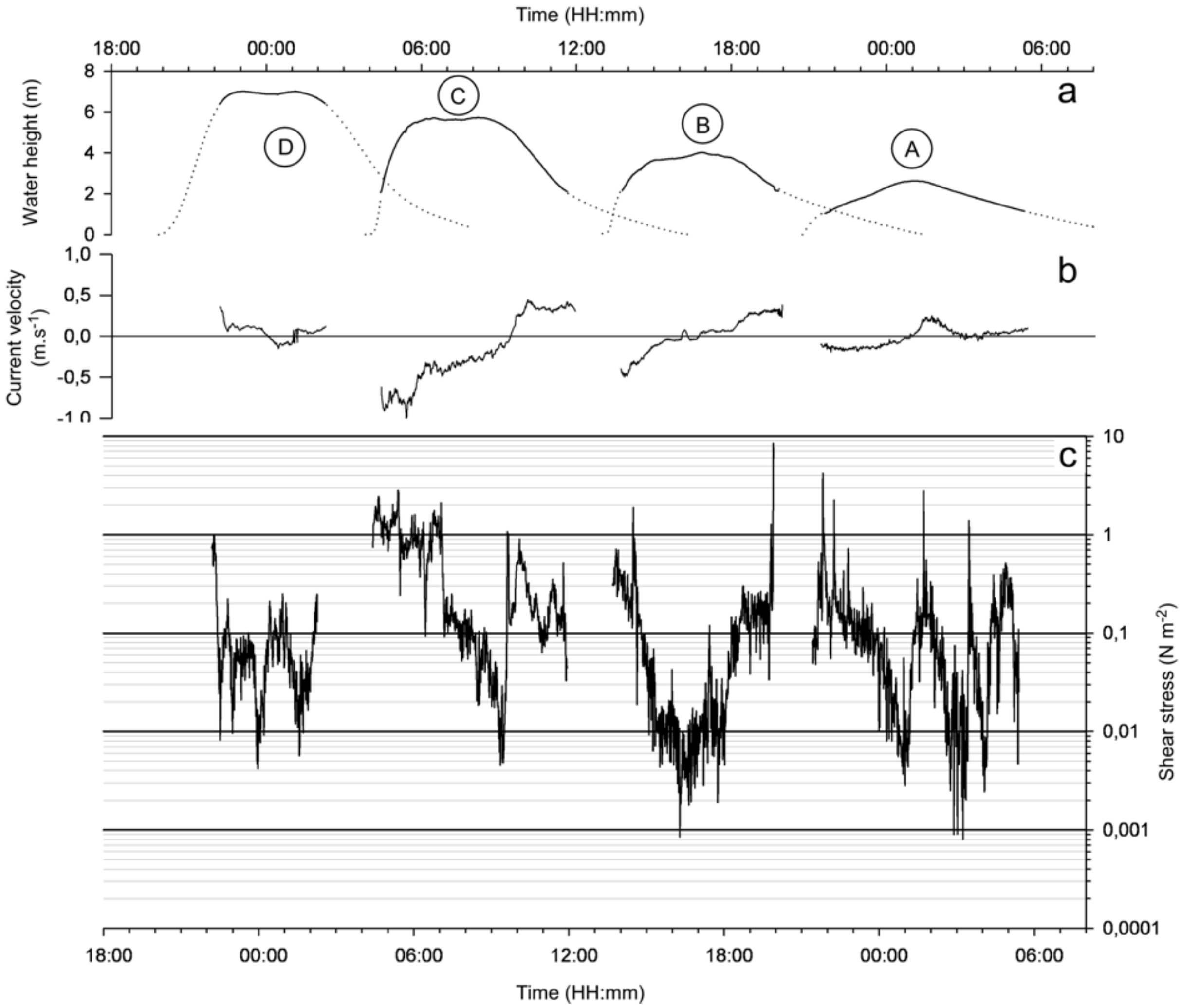

Fig. 4 - Verney et al.

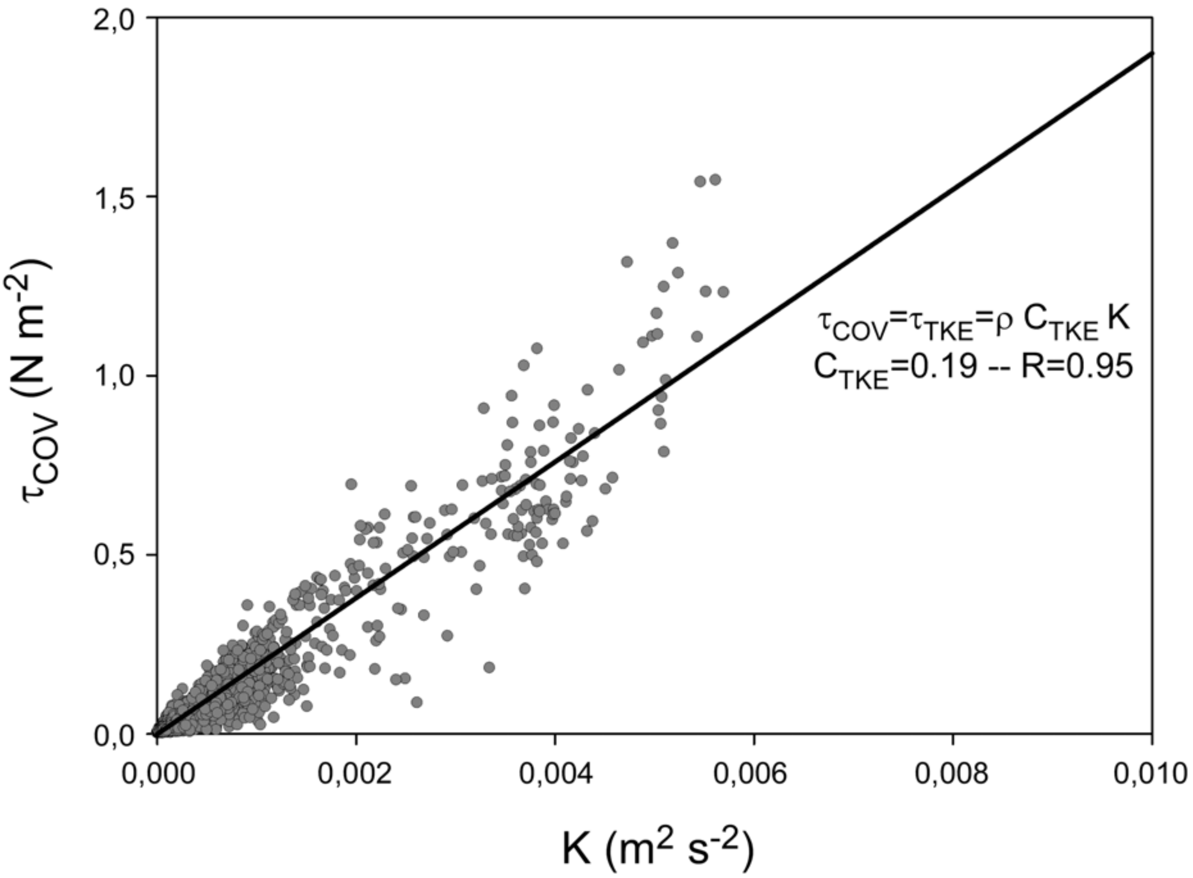

Fig. 5 – Verney et al.

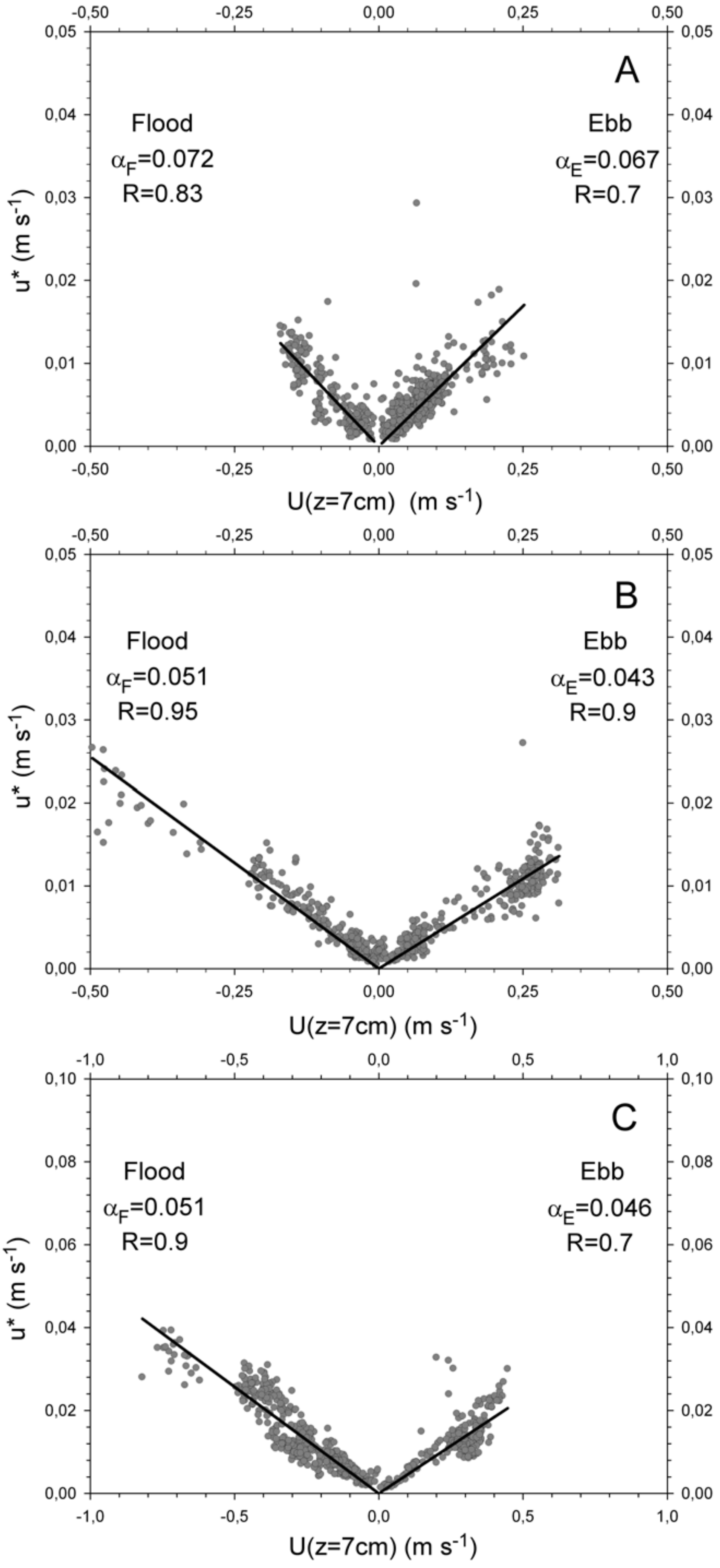

Fig. 6 – Verney et al.

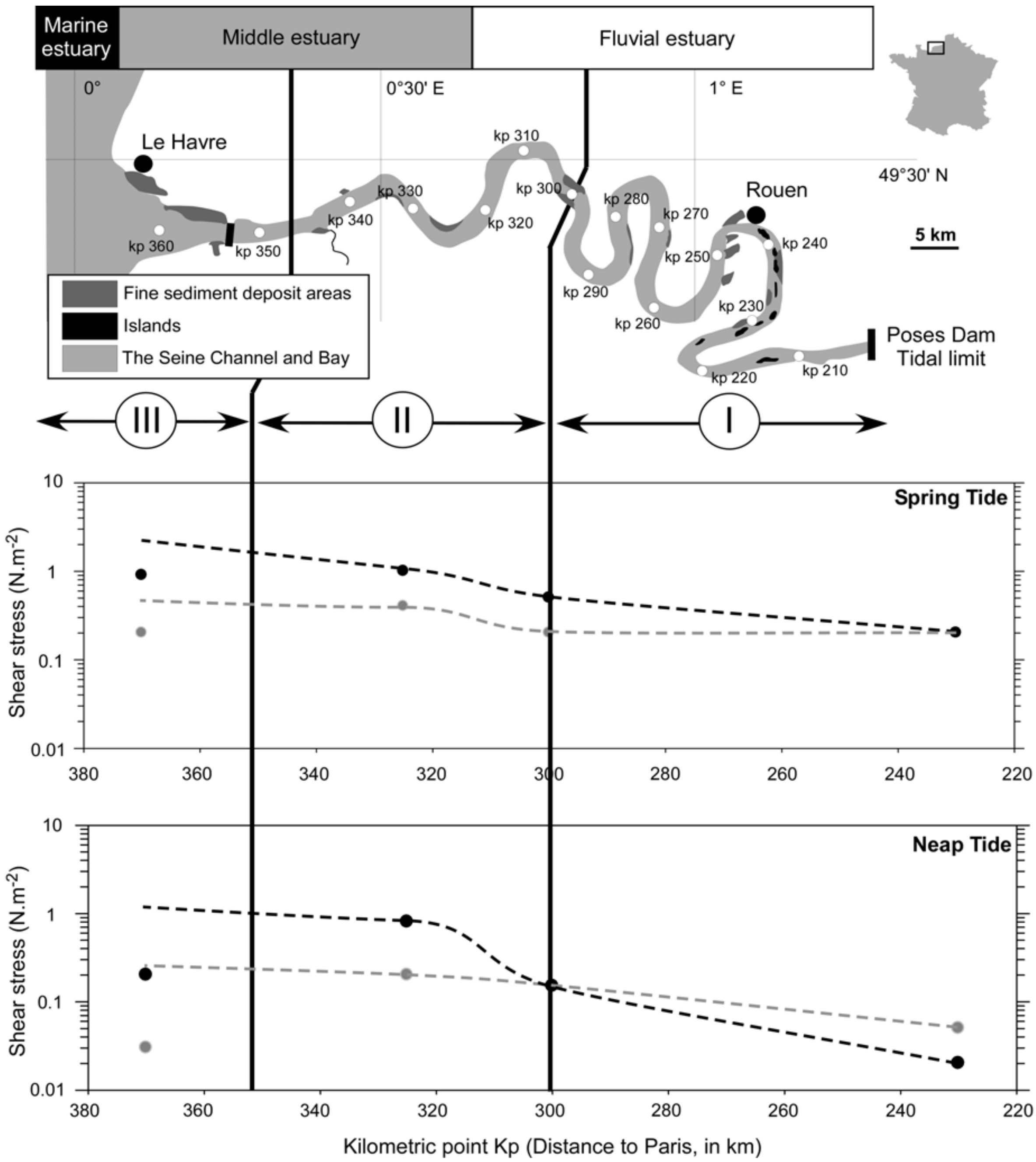

Fig. 7 – Verney et al.